



HAL
open science

Combining Landsat observations with hydrological modelling for improved surface water monitoring of small lakes

A. Ogilvie, Gilles Belaud, Sylvain Massuel, M. Mulligan, P. Le Goulven, Pierre-Olivier Malaterre, R. Calvez

► **To cite this version:**

A. Ogilvie, Gilles Belaud, Sylvain Massuel, M. Mulligan, P. Le Goulven, et al.. Combining Landsat observations with hydrological modelling for improved surface water monitoring of small lakes. *Journal of Hydrology*, 2018, 566, pp.109-121. 10.1016/j.jhydrol.2018.08.076 . hal-02608067

HAL Id: hal-02608067

<https://hal.inrae.fr/hal-02608067>

Submitted on 16 May 2020

HAL is a multi-disciplinary open access archive for the deposit and dissemination of scientific research documents, whether they are published or not. The documents may come from teaching and research institutions in France or abroad, or from public or private research centers.

L'archive ouverte pluridisciplinaire **HAL**, est destinée au dépôt et à la diffusion de documents scientifiques de niveau recherche, publiés ou non, émanant des établissements d'enseignement et de recherche français ou étrangers, des laboratoires publics ou privés.

Combining Landsat observations with hydrological modelling for improved surface water monitoring of small lakes

Andrew Ogilvie^{a,b,*}, Gilles Belaud^a, Sylvain Massuel^a, Mark Mulligan^b,
Patrick Le Goulven^a, Pierre-Olivier Malaterre^a, Roger Calvez^a

^a*G-EAU, AgroParisTech, Cirad, IRD, IRSTEA, Montpellier SupAgro, Univ Montpellier,
Montpellier, France*

^b*Department of Geography, King's College London, WC2R 2LS London, UK*

Abstract

1 Small reservoirs represent a critical water supply to millions of farmers
2 across semi-arid regions, but their hydrological modelling suffers from data
3 scarcity and highly variable and localised rainfall intensities. Increased avail-
4 ability of satellite imagery provide substantial opportunities but the moni-
5 toring of surface water resources is constrained by the small size and rapid
6 flood declines in small reservoirs. To overcome remote sensing and hydro-
7 logical modelling difficulties, the benefits of combining field data, numerical
8 modelling and satellite observations to monitor small reservoirs were inves-
9 tigated. Building on substantial field data, coupled daily rainfall-runoff and
10 water balance models were developed for 7 small reservoirs (1-10 ha) in semi
11 arid Tunisia over 1999-2014. Surface water observations from MNDWI clas-

*Corresponding author

Email addresses: andrew.ogilvie@ird.fr (Andrew Ogilvie),
gilles.belaud@supagro.fr (Gilles Belaud), sylvain.massuel@ird.fr (Sylvain
Massuel), mark.mulligan@kcl.ac.uk (Mark Mulligan), patrick.legoulven@ird.fr
(Patrick Le Goulven), pierre-olivier.malaterre@irstea.fr (Pierre-Olivier
Malaterre), roger.calvez@ird.fr (Roger Calvez)

12 sifications on 546 Landsat TM, ETM+ and OLI sensors were used to update
13 model outputs through an Ensemble (n=100) Kalman Filter over the 15
14 year period. The Ensemble Kalman Filter, providing near-real time cor-
15 rections, reduced runoff errors by modulating incorrectly modelled rainfall
16 events, while compensating for Landsat's limited temporal resolution and
17 correcting classification outliers. Validated against long term hydrometric
18 field data, daily volume root mean square errors (RMSE) decreased by 54%
19 to 31 200 m³ across 7 lakes compared to the initial model forecast. The
20 method reproduced the amplitude and timing of major floods and their de-
21 cline phases, providing a valuable approach to improve hydrological moni-
22 toring (NSE increase from 0.64 up to 0.94) of flood dynamics in small water
23 bodies. In the smallest and data-scarce lakes, higher temporal and spatial
24 resolution time series are essential to improve monitoring accuracy.

Keywords: Remote sensing, Water balance, Rainfall-runoff model, Data
assimilation, Ensemble Kalman Filter, Water harvesting

25 **1. Introduction**

26 *1.1. Hydrology of small water bodies*

27 Small reservoirs have developed across semi-arid areas to reduce transport
28 of eroded soil and mobilise water resources for local users. Their reduced
29 costs favoured significant bottom-up development, resulting in several million
30 small reservoirs worldwide (Lehner et al., 2011). Due to their modest size
31 and large numbers, field monitoring of small water bodies remains rare except
32 for scientific purposes (Albergel and Rejeb, 1997), limiting their hydrological
33 understanding.

34 Local studies in Sub-Saharan Africa (Desconnets et al., 1997; Martin-
35 Rosales and Leduc, 2003), Brazil (Molle, 1991), Mexico (Avalos, 2004), India
36 (Massuel et al., 2014b) and Tunisia (Grunberger et al., 2004; Zammouri and
37 Feki, 2005) performed water balance modelling to quantify available resources
38 and hydrological processes illustrated in figure 1. These exploit field measure-
39 ments of rainfall, reservoir stage and pan evaporation but difficulties occur
40 due to the uncertainties in estimating inflow, infiltration and groundwater
41 inflow, withdrawals and lake evaporation (Li and Gowing, 2005), which must
42 be modelled, extrapolated and/or neglected based on reasonable assump-
43 tions. Inflow due to diffuse runoff is often assessed indirectly by closing the
44 water balance or through rainfall-runoff modelling. The latter notably suffer
45 from the spatial variability of semi-arid rainfall regimes, leading to model
46 performance of NSE=0.5 or less, even with site specific field data (Lacombe
47 et al., 2008; Neppel et al., 1998; Ogilvie, 2015). Difficulties increase when
48 seeking to upscale site specific data and model water resources in ungauged
49 small reservoirs (Cudennec et al., 2007; Hrachowitz et al., 2013).

50 As a result, limited information exists on their water resources, prevent-
51 ing the optimisation of farming practices and local stakeholder investments
52 (Wisser et al., 2010). Capturing runoff and favouring evaporation and in-
53 filtration, these reservoirs also modify the spatio-temporal distribution of
54 resources. Hydrological studies have shown these can reduce downstream
55 flows by up to 80 % in small catchments and highlighted their cumulative in-
56 fluence in larger catchments (Ma et al., 2010; Nyssen et al., 2010). Studies in
57 China (Gao et al., 2011; He et al., 2003) and Tunisia (Kingumbi et al., 2007;
58 Lacombe et al., 2008; Ogilvie et al., 2016b) on catchments over 1000 km^2

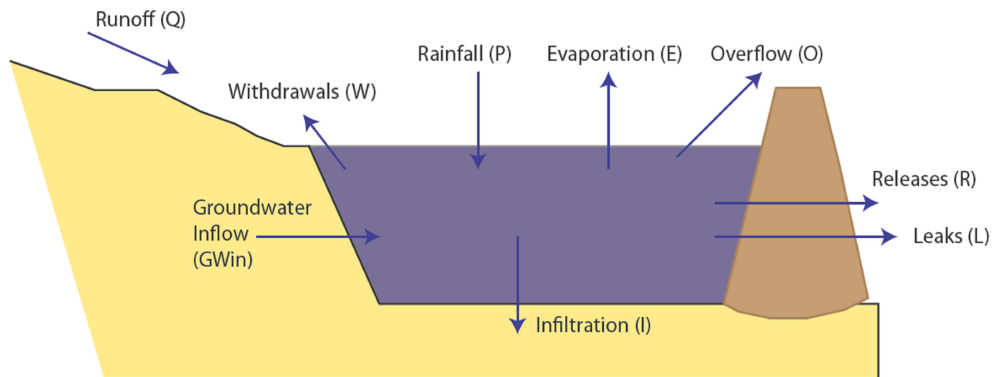


Fig. 1. Water balance fluxes in small reservoirs

59 identified reductions ranging between 1 and 50% over the same periods and
60 catchments, highlighting the uncertainties resulting in part from hydrological
61 data scarcity on small reservoirs.

62 1.2. Remote sensing and data assimilation of small water bodies

63 Satellite imagery is increasingly exploited to provide input data or to
64 calibrate hydrological models, with remotely sensed values of evaporation,
65 rainfall and soil moisture (Soti et al., 2010; Zribi et al., 2011) or assessments
66 of surface water areas (Leauthaud et al., 2013; Ogilvie et al., 2015; Swenson
67 and Wahr, 2009), lake and river stages (da Silva et al., 2014), and lake water
68 volumes (Baup et al., 2014; Crétaux et al., 2015; Frappart et al., 2018). Used
69 extensively across large wetlands, lakes or rivers, and at continental or global
70 scales, remote sensing has also been applied to provide insights across smaller
71 water bodies.

72 Studies using Landsat 30 m or pansharpned 14.5 m (Feng et al., 2016)
73 notably enabled mapping numerous water bodies and their storage capacities

74 (Liebe et al., 2005; Sawunyama et al., 2006). Long term Landsat time series
75 have also recently been used to monitor surface water variations over time.
76 Pekel et al. (2016) developed a publicly available global data set of surface
77 water at a monthly scale over 1984-2015. Ogilvie et al. (2018) showed the
78 benefits of a specific approach to monitor small reservoirs (< 10 ha) and
79 account for the greater presence of flooded vegetation (Mueller et al., 2016;
80 Yamazaki and Trigg, 2016) and difficulties resulting from limited spatial (30
81 m) and temporal resolution (up to 8 day from the combination of Landsat 8
82 and Landsat 7 satellites). These succeeded in reducing mean surface water
83 RMSE to 9 300 m² (NRMSE = 24%) but the presence of clouds reduced
84 image availability reducing the method's ability to detect rapid floods and
85 reproduce coherent flood declines.

86 Data assimilation seeks to combine external sources of data or obser-
87 vations to beneficially correct or calibrate in real time (i.e. as observations
88 become available) model outputs. Widely relied on in meteorology, it has be-
89 come increasingly used in other scientific fields, including hydrology (Beven
90 and Freer, 2001; Boulet et al., 2002; Clark et al., 2008; Emery et al., 2017;
91 Moradkhani et al., 2005; Xie and Zhang, 2010) notably to combine the bene-
92 fits of increasingly available and valuable (precise, accurate, higher temporal
93 and spatial resolution) remote sensing data.

94 To overcome the difficulties in monitoring surface water variations in small
95 reservoirs through hydrological modelling and satellite imagery, the benefits
96 of combining field data, numerical modelling and remote sensing were inves-
97 tigated here. A daily hydrological model to simulate volumetric changes in
98 small reservoirs combined with an Ensemble Kalman filter to reevaluate in

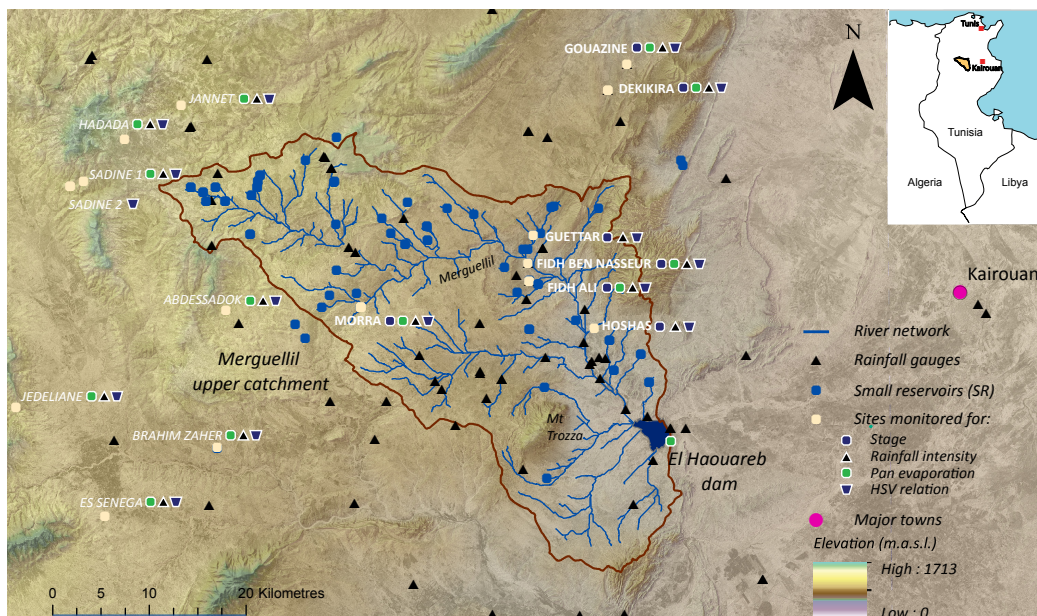


Fig. 2. Location of Merguellil upper catchment and of neighbouring hydrometeorological data used in the paper. In bold, the 7 modelled reservoirs.

99 real time model outputs based on Landsat observations was developed here.
100 The benefits of this combined model on daily values and mean annual avail-
101 ability were assessed against field data on 7 gauged reservoirs and compared
102 with results obtained using only hydrological modelling or Landsat observa-
103 tions. Finally, the sensitivity of the approach to downgrading the confidence
104 in input values and moving towards conditions found on ungauged reservoirs
105 was investigated.

106 2. Methods

107 2.1. Study sites

108 This research focussed on seven small reservoirs in semi-arid central Tunisia
109 (figure 2) benefiting from long term hydroclimatic data acquired through re-

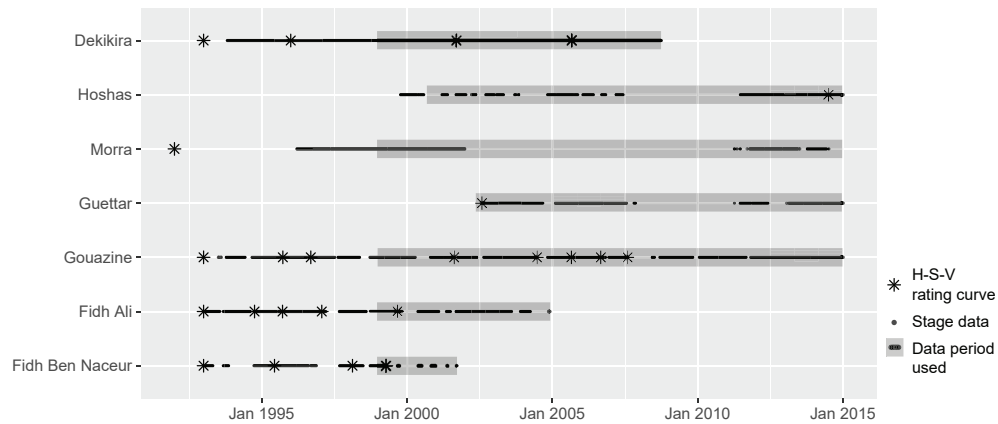


Fig. 3. Availability of stage field data and rating curves over modelling periods of the 7 lakes

110 search collaboration with government agencies (Albergel and Rejeb, 1997;
 111 Leduc et al., 2007; Ogilvie, 2015). Field instrumentation on each lake con-
 112 sisted of automatic stage pressure transducers and tipping bucket rainfall
 113 gauges, supplemented by daily limnimetric (ladder) and rainfall readings by
 114 local observers. Thirteen lakes in the vicinity had also been equipped with
 115 evaporation pans. Complementary pressure transducers and automatic rain-
 116 fall gauges were installed as part of this research in 2011 on three lakes
 117 (Hoshas, Morra, Guettar) to extend time series (figure 3) and tend to the
 118 declining monitoring network exacerbated by the Tunisian revolution.

119 Stage and surface area were converted using site specific Height-Surface-
 120 Volume relations (figure 3) acquired and updated since the 1990s to account
 121 for silting (Albergel and Rejeb, 1997). Complementary surveying was also
 122 carried out on Hoshas in 2014. Figure 4 illustrates the shift in the rating
 123 curves from silting, which can be used to assess the level of uncertainty
 124 associated with volumes in recent years. On Gouazine, after 6 years (2001

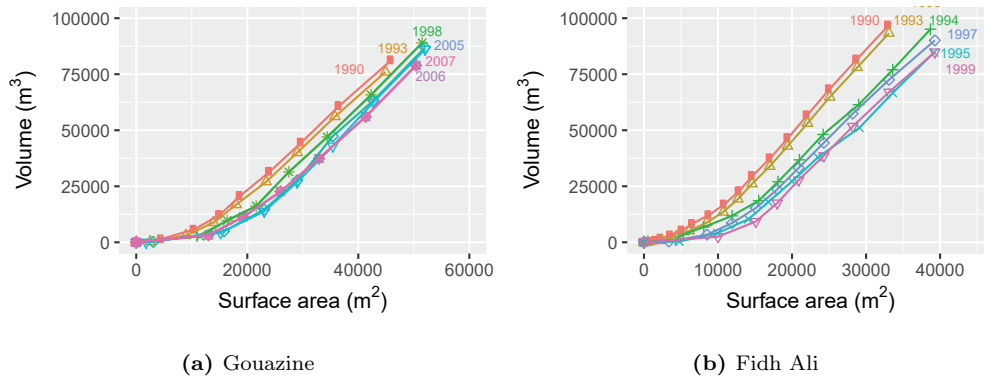


Fig. 4. Change over time of surface area - volume rating curves for two small lakes

125 vs. 2007) the obsolescence of the rating curve results in a mean RMSE
126 of $4900 m^3$, while on Fidh Ali it reaches $25\ 000 m^3$ on volumes under $80\ 000 m^3$.
127 $000 m^3$. On lakes where rating curves could not be updated (Guettar and
128 Morra) for logistical reasons (cost, access to lakes and presence of water
129 and/or vegetation on lake bed), GPS contours nevertheless highlighted that
130 errors in the H-S rating curves only reached 11-12% after 12 and 22 years
131 respectively (Ogilvie et al., 2018).

132 These are inferior to errors generated from extrapolating capacity loss
133 based on studies on 15 nearby surveyed reservoirs (figure 2), due to the
134 strong disparities in silting rates and the difficulties in erosion modelling,
135 especially over extended periods (Albergel and Rejeb, 1997; Baccari et al.,
136 2008; Hentati et al., 2010; Lacombe, 2007; Ogilvie, 2015). The Gouazine
137 reservoir benefited from the longest and most reliable time series (figure
138 3) due to regular maintenance, field observations and six updates to the
139 stage-surface-volume rating curves but results on other reservoirs enabled to
140 confront the method on lakes of different capacities ranging between $50 m^3$

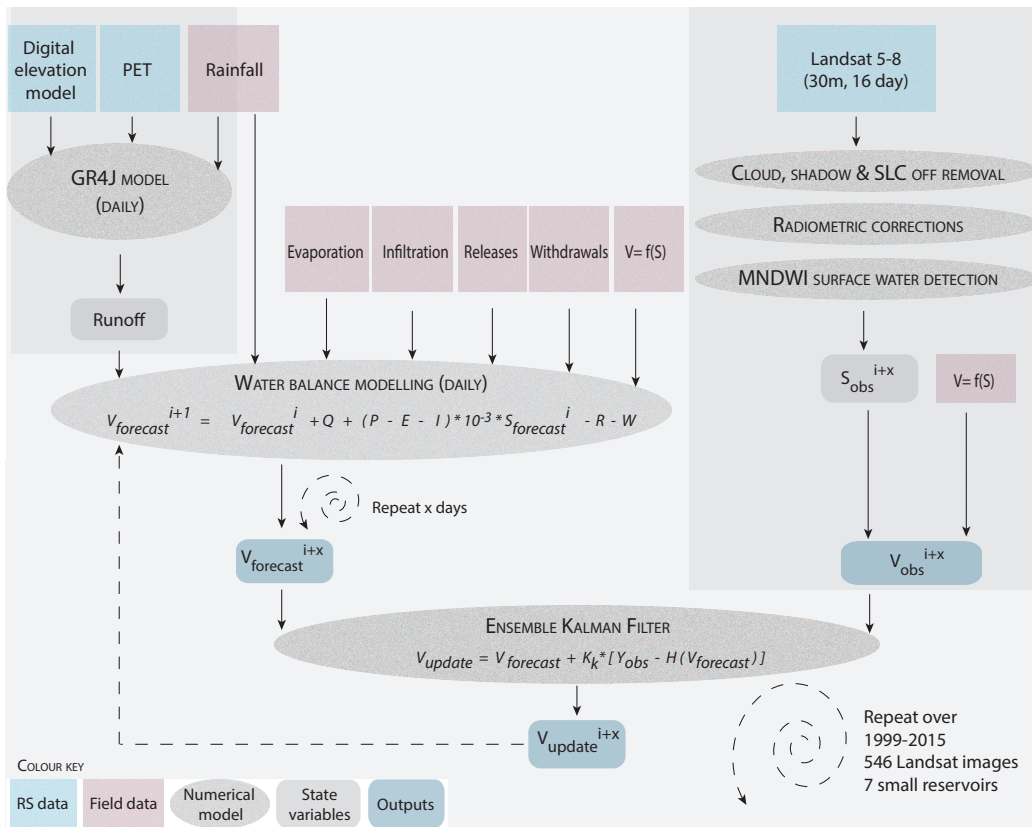


Fig. 5. Schematic representation of methodology for assimilation of Landsat observations into hydrological model with the Ensemble Kalman Filter

141 and 700 000 m³ (table 1).

142 The field data collected were used to estimate the multiple fluxes in the
 143 water balance (WB) of small lakes and develop rainfall-runoff models for their
 144 catchments. Site specific hydrological models were developed over 1999-2014
 145 for seven lakes, before evaluating the benefits of integrating earth observation
 146 data, as illustrated in figure 5.

147 *2.2. Water balance modelling of 7 small water bodies*

148 *2.2.1. Rainfall inputs*

149 Daily rainfall (P , mm/day) over the 7 lakes was interpolated over 1999-
150 2014 from the 50 manual and automatic rainfall gauges situated at the lakes
151 and within and around their catchments (figure 2). Inverse Distance Weight-
152 ing (IDW) interpolation was used after tests showed the marginal benefit
153 (error reduction by 1 mm) (Ogilvie, 2015) of geostatistical methods such
154 as Kriging with external drift (Hengl et al., 2007) compared to the lengthy
155 treatment times. Mean rainfall varied between 299 mm/year \pm 108 mm/year
156 to 396 mm/year \pm 124 mm/year (table 1). The homogeneous distribution of
157 the rainfall gauges in this catchment inherently accounts for the altitudinal
158 gradient within subcatchments (Feki et al., 2012; Ogilvie et al., 2016b; Van
159 Der Heijden and Haberlandt, 2010; Wackernagel, 2004).

160 *2.2.2. Lake evaporation*

161 Lake evaporation rates (E , mm/day) were IDW interpolated based on
162 field observations from Colorado type sunken pans on 13 lake shores over
163 1999-2008 (figure 2). Evaporation time series were completed to 2015 based
164 on linear regressions between each lake and a reference station with contin-
165 uous observations (El Haouareb), assuming homogeneous evaporation varia-
166 tions across the basin ($R^2 = 0.92$). Potential lake evaporation varied across
167 lakes between 1776 mm/year \pm 143 mm/year to 2019 mm/year \pm 198 mm/year
168 (table 1). A pan coefficient (C_t) of 0.8 based on water bodies of similar sizes
169 in semi-arid areas was used (Alazard et al., 2015; Cadier, 1996; Linacre, 1994;
170 McMahon et al., 2013; Molle, 1991; Riou, 1972).

171 *2.2.3. Infiltration rules*

172 Infiltration (I , mm/day) was modelled based on equation 1 where Z_{water}
173 is the absolute head of water (mm), a the slope, and i_0 (mm/day) the inter-
174 cept values provided in table A.1. These were extracted from Lacombe (2007)
175 and estimated for Guettar, Dekikira and Hoshas (figure 6) during depletion
176 phases (respectively 1262, 651 and 1546 days) when other fluxes are absent
177 (rainfall, runoff, withdrawals, releases) based on stage monitoring and esti-
178 mated evaporation (Lacombe, 2007; Ogilvie, 2015). Mean daily infiltration
179 varied between 2 mm and 28 mm for a lake on gravely soil (table 1). Re-
180 cent data do not indicate a noticeable change in infiltration properties from
181 silting over time, confirming past observations (Lacombe, 2007). Similarly,
182 uncertainties from silting on the absolute head of water used in infiltration
183 rules are estimated on average at 12.5% per metre, and may be lower due
184 to partial silting of the lake floor and constant infiltration rates observed
185 on four of these lakes (Ogilvie, 2015). Groundwater and subsurface inflow
186 are often neglected in water budgets (Lacombe, 2007; Li and Gowing, 2005)
187 as these are minor fluxes and their quantification requires intense monitor-
188 ing and geochemical methods (Massuel et al., 2014b; Montoroi et al., 2002).
189 Accordingly, infiltration estimates provided here may in some cases corre-
190 spond to the combination of infiltration, leaks and groundwater inflow. On
191 Gouazine, groundwater inflow was shown to reach 50 m³/day (Grunberger
192 et al., 2004), meaning absolute infiltration may be up to 2.5 mm/day greater
193 when the lake is 2 ha and less when surface area rises (Ogilvie, 2015).

$$I = i_0 + a * Z_{water} \quad (1)$$

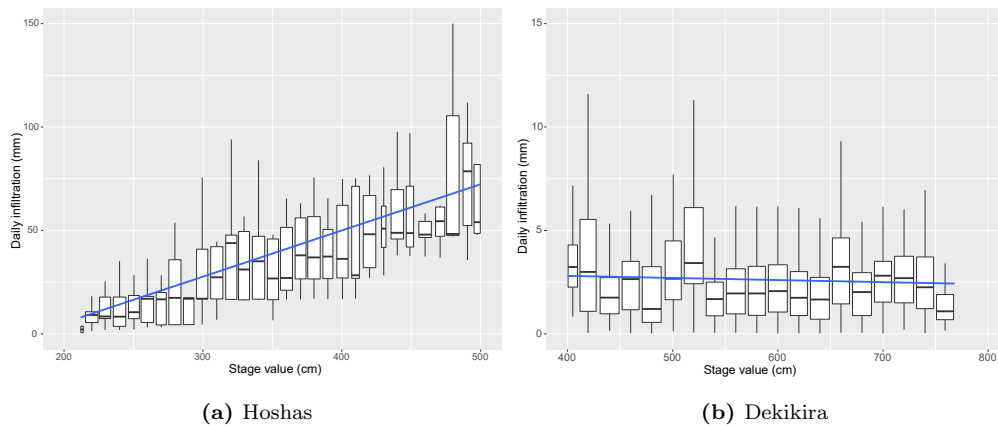


Fig. 6. Infiltration values as a function of stage in the lake estimated during depletion periods

194 *2.2.4. Modelling releases and overflows*

195 Semi-structured interviews with the dam operators revealed the absence
196 of strict rules to protect the infrastructure as releases depended on further
197 storm forecasts, government advice, presence of lakes downstream, techni-
198 cal problems with the valve and pressure from users to maintain maximal
199 resources for the dry season (Ogilvie, 2015). Releases (R , m^3/day) were de-
200 tected on two lakes after only the most significant events (1% of all events).
201 Based on the extraordinary decline rates witnessed in instantaneous (15 min)
202 hydrometric data, releases were modelled on the basis of a $10\,000\text{ m}^3/\text{day}$
203 release to reach 80% of V_{max} if and when the latter is exceeded (Lacombe,
204 2007; Ogilvie, 2015). This also accounts for overflows through the spillway.
205 Minor releases to flush out sediments and vegetation from the conduit were
206 increasingly rare and remain of the order of $1000\text{-}5000\text{ m}^3/\text{year}$.

Table 1: Characteristics of the 7 small reservoirs modelled and their catchments

Lake	Catchment size (km ²)	Altitude (m)	Initial capacity (10 ³ m ³)	Rainfall (mm/year, 1999-2014)	Evaporation (mm/year, 1999-2014)	Infiltration (mm/day, 1999-2014)
Dekikira	3.31	406	219	396	1842	2.7
Hoshas	7.90	306	130	302	2003	28
Guettar	4.98	393	150	339	1994	10
Gouazine	16.64	397	237	387	1776	9
Fidh Ali	2.74	350	134	324	2019	3.6
Fidh Ben Nasseur	1.82	368	47	327	2016	7.8
Morra	11.69	588	705	299	1917	2

207 *2.2.5. Modelling withdrawals*

208 Regular field visits and quantitative questionnaires with 48 farmers on 22
209 lakes (Ogilvie, 2015) revealed the extreme heterogeneity of pumping practices
210 across lakes and years but highlighted the absence, or reduced importance
211 of withdrawals (W , m³/day) on most lakes. These represented less than 40
212 m³/day in the summer months, compared to the 340 m³/day from infiltration
213 (of 7 mm) and evaporation (10 mm) on a small (2 ha) surface area (Lacombe,
214 2007; Ogilvie, 2015). On Guettar and Morra lakes however, withdrawals to
215 water fruit trees were estimated to reach over 130 m³/day over April to
216 October. No withdrawal restrictions to preserve the resource as it wanes
217 were observed and thus modelled (Ogilvie, 2015).

218 *2.3. Runoff estimation through GR4J catchment modelling*

219 Runoff (Q , m³/day) into small reservoirs was assessed using a daily GR4J
220 rainfall-runoff model developed for each reservoir's catchment. This lumped
221 conceptual model is well suited to the relative scarcity of data and used

222 across semi-arid catchments of comparable size (Perrin et al., 2003). A daily
223 time step was used to capture the intense rainfall events and corresponds
224 to the available rainfall and runoff data, as availability of sub-daily data
225 is extremely limited. It relies on a simple two reservoir structure and four
226 parameters:

- 227 • $X1$ production store capacity (mm)
- 228 • $X2$ groundwater exchange coefficient (mm/day)
- 229 • $X3$ routing store capacity (mm)
- 230 • $X4$ unit hydrograph time constant (day)

231 Input variables consist of catchment size delineated using 1 arc second
232 SRTM digital elevation model, rainfall (P , mm/day) IDW interpolated from
233 available observations across over 50 gauges (figure 2) and potential evapo-
234 transpiration (PET , mm/day) interpolated from 180 MODIS-derived 1 km²
235 monthly tiles. These MOD16 datasets exploit global weather data sets com-
236 bined with MODIS derived land cover types, leaf area index and albedo (Mu
237 et al., 2011) to provide monthly PET estimates, at a higher resolution than
238 the 0.5 ° Climate Research Unit products.

239 Models were calibrated using an objective function of maximal Nash Sut-
240cliffe Efficiency (NSE) on runoff. Q_{obs} was estimated based on stage mon-
241 itoring (figure 3) and a simplified water balance equation, as diffuse sheet
242 runoff and subsurface runoff prevent direct observations (Albergel et al.,
243 2003; Lacombe et al., 2008). Several fluxes can be neglected (groundwater

244 inflow, leaks) or assumed null (e.g. withdrawals) during the violent Horto-
245 nian runoff events resulting from limited vegetation, low soil water holding
246 capacities, prominent topography and high rainfall intensity characteristic
247 of Mediterranean climates (Lacombe et al., 2008). The other water balance
248 fluxes (P , E , I , releases, overflows) were assessed based on local monitoring
249 and observations as described previously. The airGR code (Coron et al.,
250 2017) which allowed for integrated numerical modelling and remote sensing
251 processing in R, as well as superior results thanks to the HBAN optimisation
252 function, was used.

253 *2.4. Combining remote sensing observations and hydrological modelling*

254 *2.4.1. Landsat surface water observations*

255 The remote sensing observations employed in the Ensemble Kalman Filter
256 were Landsat-derived surface water areas for each lake over 1999-2014. 526
257 Landsat 5-8 images available freely from USGS were corrected to surface
258 reflectance and filtered to remove acquisitions with excessive clouds, shadows
259 and inactive Scan Line Corrector (SLC-off) pixels over each lake. Flooded
260 areas were extracted using the Modified Normalised Difference Water Index
261 (Xu, 2006) calibrated against extensive field data. Full details of the approach
262 are available in Ogilvie et al. (2018) and led to a mean surface area RMSE
263 of 9 300 m². Surface areas were converted to volumes using the available
264 rating curves and values were linearly interpolated to provide a continuous
265 time series and allow comparisons with field data (V_{field}) and the Ensemble
266 Kalman Filter (V_{ENKF}) outputs. Alternate interpolation approaches (Forkel
267 et al., 2013) to gap fill and smooth daily time series failed here to provide
268 significant benefit, partly due to the abrupt fluctuations observed contrasting

269 with gradual seasonal flood pulses in larger water bodies (Leauthaud et al.,
270 2013; Ogilvie et al., 2015).

271 2.4.2. Ensemble Kalman Filter

272 Ensemble Kalman Filtering (ENKF, Evensen (2003)) is a stochastic data
273 assimilation method suited to smaller scale non-linear systems, including
274 where initial states are highly uncertain (Gillijns et al., 2006) as may be the
275 case due to poor rainfall-runoff modelling of intense rainfall events. It also
276 reduces the difficulties associated with developing a tangent linear model and
277 deriving its *adjoint* counterpart (Vermeulen and Heemink, 2006), required in
278 variational data assimilation (e.g. 3D-Var, 4D-Var), widely used in the mod-
279 elling of large systems such as atmospheric circulation models, oceanography,
280 and more recently in hydrology and hydraulics applications (Oubanas et al.,
281 2018).

282 With the Kalman filter, an initial forecast is updated using the Kalman
283 gain when an external observation is available, based on the following equa-
284 tions:

$$V_{update} = V_{forecast} + K_k * [Y_{obs} - H(V_{forecast})] \quad (2)$$

$$Y_{obs} = H(V_{obs}) + v_k \quad (3)$$

285 where K_k is the Kalman gain defined as:

$$K_k = Cy * H^T * (H * Cw * H^T + Cv)^{-1} \quad (4)$$

286 $V_{forecast}$ is here the lake volume outputted by our daily hydrological model
287 $f(V)$ with a random error w_k .

$$V_{forecast} = f(V) + w_k \quad (5)$$

288 H , called the observation operator, is the model to convert observed state
289 variables to observations. Where observations are directly inputted, as in
290 this case, $H = \text{Id}$ (identity) and equations simplify as below (equations 6
291 and 7). The external observation is the remotely sensed lake volume based
292 on Landsat imagery (V_{RS}) which have an associated random error v_k .

$$K_k = Cy * (Cw + Cv)^{-1} \quad (6)$$

$$V_{update} = V_{forecast} + K_k * [V_{obs} + v_k - V_{forecast}] \quad (7)$$

293 which can here be rewritten as:

$$V_{ENKF} = K_k * (V_{RS} + v_k) + (1 - K_k) * V_{WB+GRAJ} \quad (8)$$

294 The forecast step is repeated on a daily basis and $V_{forecast}$ is updated
295 when acceptable Landsat observations are available (equation 8). The up-
296 dated volume (V_{ENKF}) is then fed back into the daily hydrological model
297 and sequentially updated over 1999-2014 with the valid remote sensing (RS)
298 observations (figure 5).

299 Cv is the observation error covariance matrix, Cw is the forecast error
300 covariance matrix and Cy is the cross covariance matrix between the state
301 variable and the forecast. As the state variable used is the volume and not

302 an intermediary state variable, Cy is equivalent to Cw . Cv and Cw values
303 were estimated using the covariances of errors between stage observations
304 and remote sensing observations and between stage and model outputs re-
305 spectively. Stage related volumes include their own element of error (ladder
306 readings, rating curve imprecisions and evolving flood bed topography) but
307 here these are neglected compared to the errors from remote sensing (incl.
308 radiometric corrections, detection errors) and hydrological modelling. Cw
309 variance was 20 times greater than Cv variance and contributed to attribut-
310 ing greater confidence to the Landsat values over the model outputs in the
311 Kalman filtering. Alternate combinations were tested but these did not lead
312 to performance improvements. Cw remained constant as recommended by
313 Clark et al. (2008), allowing the method to be used on periods and lakes with
314 non-continuous ground truth data.

315 In the Ensemble version of the Kalman filter, n values of the initial state
316 are generated and each ensemble member is run through the forecast and
317 update step. The n values of the initial state are generated based upon a
318 random synthetic error y so that values have mean value initial state and
319 predefined covariance Cy . Initial states are the same as V (equation 5) and
320 not an intermediary variable, so y was taken to be w_k , the forecast error
321 (Moradkhani et al., 2005). The n ensemble of external observations are
322 generated randomly to obtain a normal (Gaussian) distribution with error
323 v_k , i.e. centred on the observation value and with predefined covariance Cv
324 (Reichle et al., 2002). Here $n = 100$, as Gillijns et al. (2006) reveal marginal
325 benefits above 100 and greater errors for n values below 40.

326 *2.5. Performance and sensitivity of the ENKF approach*

327 The performance of the Ensemble Kalman Filter (V_{ENKF}) was assessed
328 against available field data (V_{field}) and compared with the performance of
329 using only hydrological model ($V_{WB+GR4J}$) and only remote sensing (V_{RS})
330 data. NSE values were calculated but considering their sensitivity to tim-
331 ing of outputs and ability to disguise certain errors (Moussa, 2010), RMSE
332 values were provided. The performance in terms of individual daily volumes
333 was investigated as well as on annual water availability, considering their
334 importance to local users.

335 The method's performance, as inputs and parameters were degraded, was
336 then tested on four lakes to study its sensitivity and identify the ability of
337 RS observations to correct for greater uncertainties. The influence of re-
338 duced rainfall observation networks was considered, based on rainfall time
339 series interpolated after artificially removing gauges in the catchment. In-
340 formation gathered across 15 gauged reservoirs was also used to consider
341 the applicability of the approach to nearby ungauged catchments based on
342 average infiltration rules, transposing GR4J parameters and modeling an av-
343 erage surface volume power relation adapted for silting over time detailed in
344 Ogilvie et al. (2016a).

345 **3. Results and discussion**

346 *3.1. Hydrological modelling of small water bodies*

347 Figure 7 illustrates the daily volume dynamics on lake Gouazine simulated
348 by the hydrological model. Compared to the long term field observations,

349 results highlight the ability of the model to reproduce coherent flood dy-
350 namics and declines rates, for floods of varying amplitudes. Flood peaks
351 were however, in some cases, under and over estimated as in 2003 (-54%) or
352 2007 (+198%) according to field data on lake Gouazine. Difficulties occurred
353 due to the low performance of the GR4J rainfall-runoff model, where NSE
354 reached values around 0.5-0.6 on Gouazine and Dekikira, but nearer 0.2-0.3
355 on other lakes (table 2), notably on lakes with less extensive and reliable field
356 data (rainfall, stage and rating curves). Though low, these are comparable
357 to previous GR4J results in the basin (Lacombe, 2007) and due largely to
358 insufficient rainfall gauge densities which fail to capture the high intensities
359 of very localised rainfall events (Neppel et al., 1998).

360 *3.1.1. Rainfall-runoff modelling limitations*

361 To simulate the uncertainties from the absence of upstream rainfall gauges
362 in the catchments of small reservoirs, rainfall was interpolated for the Gouazine
363 catchment after artificially excluding its upstream gauge data. IDW interpo-
364 lated rainfall was then underestimated by 20.3% on 44 out of 53 events over 20
365 mm. The performance of the GR4J model decreased marginally (NSE=0.55),
366 however for the combined WB+GR4J model NSE declined from 0.57 to 0.24,
367 due to the knock on effect of errors during the flood decline (e.g. floods
368 missed in 2012 and 2014 in figure 12). Conversely, rainfall underestimation
369 forced the model during calibration to increase runoff coefficients, leading to
370 overestimation on other events which had been accurately detected due to
371 their larger spatial extent. These results highlight the importance of reli-
372 able upstream gauges to detect orographic rainfall intensities and the order
373 of magnitude of uncertainties in catchments where upstream stations are

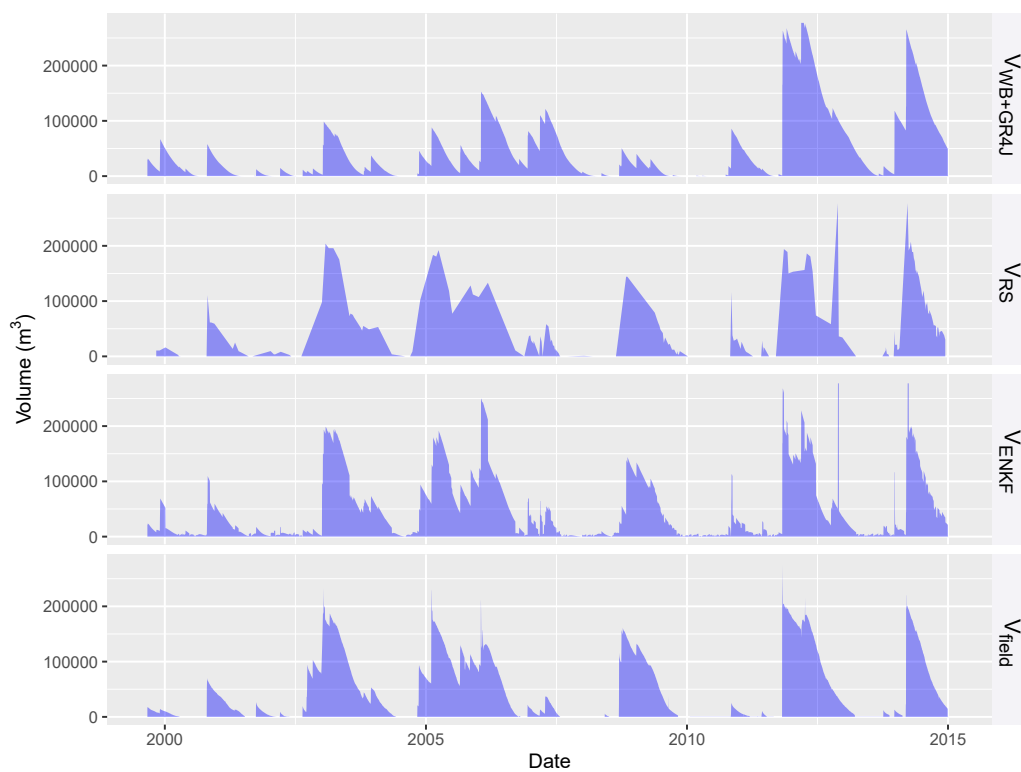


Fig. 7. Comparing observed daily volumes (V_{field}) for Gouazine lake, 1999-2014 with values obtained by the hydrological model ($V_{WB+GR4J}$), the remote sensing observations (V_{RS}) and their combination through Ensemble Kalman Filtering (V_{ENKF})

374 unavailable (i.e. all here, except Gouazine).

375 Even with an upstream station, certain events were underestimated on
376 Gouazine (in 2003, 2005, and 2009 on figure 7) due to undetected localised
377 storm cells. At the event scale, altitude variograms (e.g. KED) were not suffi-
378 cient either to correctly modulate over space the amplitude of events. Though
379 meteorological satellite observations (e.g. TRMM) do not provide reliable es-
380 timates at the event scale on such small catchments ($< 20 \text{ km}^2$), these or even
381 phone signal networks (Doumounia et al., 2014; Overeem et al., 2013) may
382 help define variograms and improve geostatistical interpolation. In larger
383 catchments or where the density of observations is greater, distributed mod-
384 els may also help account for space-time rainfall variability (Aouissi et al.,
385 2018).

386 Errors from the limited rainfall gauge density were further exacerbated
387 by inherent measurement gaps and errors due to equipment malfunctions
388 (obstructions, low maintenance) and the absence of sub-daily time series to
389 capture the flood peak accurately. Though 93% of storms over 10 mm were
390 separated by 24 hours (Lacombe, 2007), certain large events were poorly
391 modelled as substantial rains scattered over successive days, led to very high
392 runoff on the third day only, due to saturated soils and delayed subsurface
393 flows, causing calibration difficulties. Furthermore, the volume of the first
394 storms can be overestimated due to silting, and because ladders rarely moni-
395 tor the lowest stage levels, due to logistical reasons of installation and regular
396 access.

397 *3.1.2. Heterogeneous catchment responses*

398 The low GR4J performance partly translated difficulties to model the
399 catchment's response. The intensity but also land cover, antecedent soil
400 humidity or conservation works such as contour benches can significantly in-
401 fluence runoff coefficients in these catchments as discussed in (Ogilvie et al.,
402 2016b). Model parameter $X1$ notably seeks to account for the soil humidity
403 and the threshold effect, leading to greater runoff once $X1$ is saturated. The
404 lumped (i.e. not spatialised) nature of the GR4J model makes accounting
405 for localised changes in catchment behaviour (water conservation works, land
406 cover and cropping) difficult however. Model choice guided by limited data
407 availability precluded the selection of a more data intensive semi-distributed
408 and/or physical model capable of accounting for discrete changes over time
409 in land cover and land use. Changing model parameters over time can al-
410 ternatively indirectly account for this but only at the catchment scale. On
411 Gouazine, where numerous studies discuss the possible reduction in runoff
412 from the development of contour benches on 43% of its catchment area (Nasri,
413 2007), calibrating over 1997-2003 led to a routing store capacity ($X3$ param-
414 eter) 5 times greater than over the whole period, possibly pointing to the
415 greater retention capacity from water soil and conservation works. Model
416 performance improved (NSE rose to 0.67) but only marginally as it remained
417 affected by the other difficulties discussed above.

418 *3.2. Combining remote sensing and hydrological modelling*

419 *3.2.1. Ensemble Kalman filter performance on daily volumes*

420 Figure 7 compares the daily volume dynamics on lake Gouazine based on
421 outputs from the hydrological model, the remote sensing observations, and

422 their combination through the Ensemble Kalman filter. Remotely sensed
423 volumes provided greater accuracy in the estimations of flood peaks than
424 the hydrological model however outliers remained present (e.g. 2006 and
425 2013). Furthermore, the low frequency of acceptable observations (on average
426 1.5/month) led to poor representation of the rapid flood rises as in 2003
427 (Ogilvie et al., 2018).

428 The Ensemble Kalman filter improved the performance of the site-specific
429 hydrological models, with Landsat observations notably modulating the ini-
430 tial $V_{WB+GRAJ}$ forecast and usefully correcting the flood peaks under and
431 overestimated by the model (figure 7). These errors were carried through the
432 decline phase of the hydrological models and figure 8 clearly illustrates the
433 correction from the satellite observation which draws volumes closer to the
434 1:1 line, raising the NSE value, for instance from 0.57 to 0.81 on Gouazine.
435 This effect was pronounced on larger lakes that do not dry out, as overes-
436 timations in the model outputs led to a progressive drift, which the ENKF
437 usefully corrected (figure 9).

438 Accordingly, RMSE (table 2) reduced thanks to the Landsat corrections
439 on 5 of the lakes (Dekikira, Gouazine, Fidh Ali, Morra and Guettar). Mean
440 RSME reduced by 54% to 31 200 m³ across all lakes and 21 400 m³ when
441 excluding the much larger dam (Morra). Compared to the range of flood val-
442 ues experienced by these lakes, NRMSE reached an acceptable 0.26. Greater
443 errors were observed due in part to reduced model performance, preponder-
444 ant remote sensing uncertainties (e.g. Hoshas) and less reliable hydrometric
445 field data (HSV on Morra and Guettar). The lower NSE on the smallest
446 reservoirs (Hoshas, Fidh Ben Nasseur) were to be expected here considering

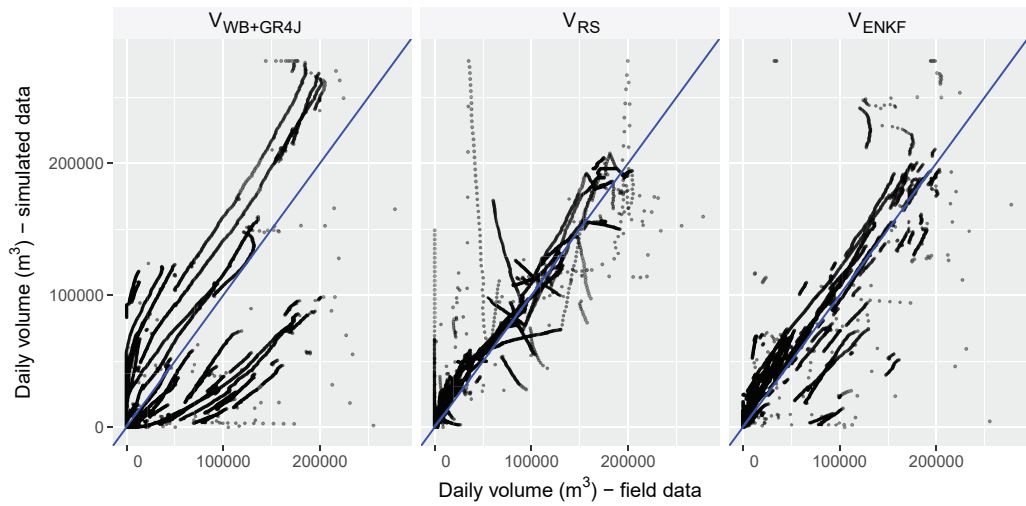


Fig. 8. Scatterplot between modelled and observed daily volumes on lake Gouazine, 1999-2014

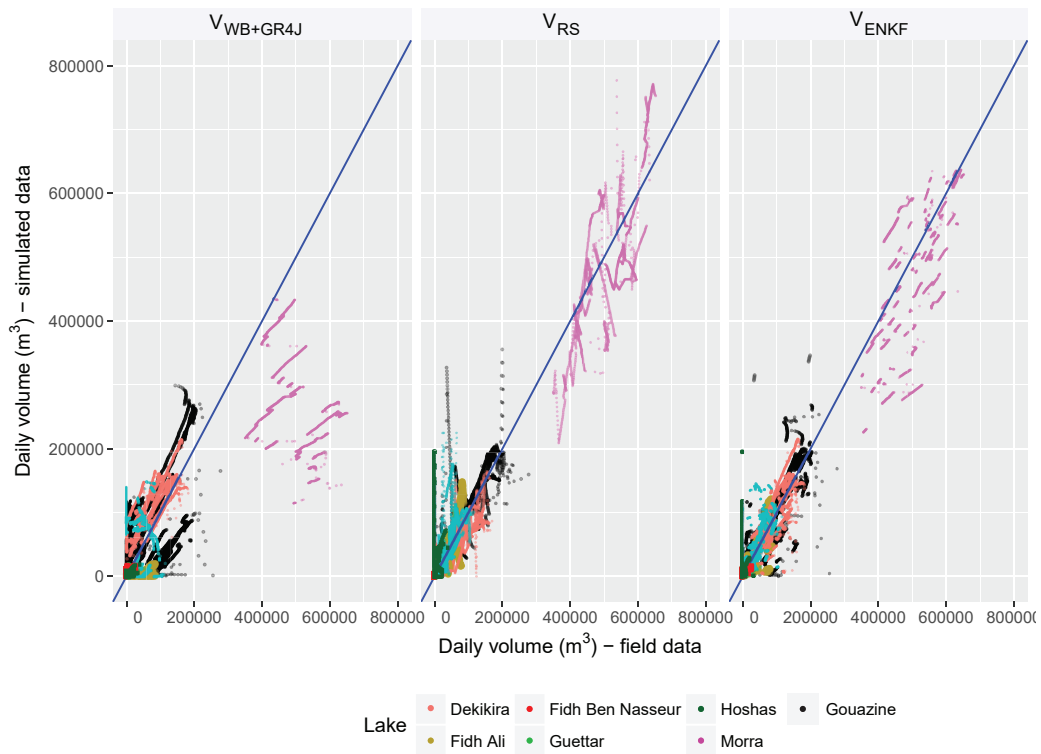


Fig. 9. Scatterplot between modelled and observed daily volumes for all 7 lakes, 1999-2014

447 the spatial resolution (30 m) of satellite imagery used here and the mean
448 flooded surface area around 1000 m² (Ogilvie et al., 2018).

449 Remote sensing observations are capable of representing flood dynamics
450 with low RMSE but suffer from overclassifications due to undetected clouds
451 and from the reduced temporal resolution of Landsat imagery (on average 1.5
452 image/month due to clouds) (Ogilvie et al., 2018). The ENKF approach de-
453 veloped here enabled remote sensing outliers to be rapidly corrected here, as
454 seen on Gouazine in 2012 (figures 7 and 8) and Morra (figure 9) for instance.
455 The combination with rainfall-runoff modelling also reduced interpolation er-
456 rors resulting from insufficient observations close to the flood peak as seen on
457 figure 7. Similarly, the ENKF also helped identify additional flood peaks as
458 in 2006. Over long periods, ENKF led to a reduction of RMSE near 10% on
459 Dekikira and Guettar. Large errors in the initial forecast led to marginally
460 higher RMSE with ENKF than V_{RS} on some lakes. However, as seen in figure
461 7, the ENKF approach enabled a more coherent and accurate reproduction
462 of daily flood dynamics even on these lakes. Over a single hydrological year,
463 the reduction in RMSE from ENKF over interpolated remote sensing obser-
464 vations also reached up to 46% on Gouazine.

465 3.2.2. Ensemble Kalman Filter performance on annual water availability

466 The method's performance in assessing annual water availability rather
467 than fine flood dynamics (i.e. individual observations) is shown in figures 10
468 and 11, and summarised in table 3. The ENKF method improved on the
469 initial $V_{WB+GR4J}$ results (NSE=0.62), except on the smallest lakes (Hoshas
470 and Fidh Ben Nasseur). Nevertheless, the orders of magnitude of the ENKF
471 estimated volumes on Hoshas (figure 10) remain correct in comparison to

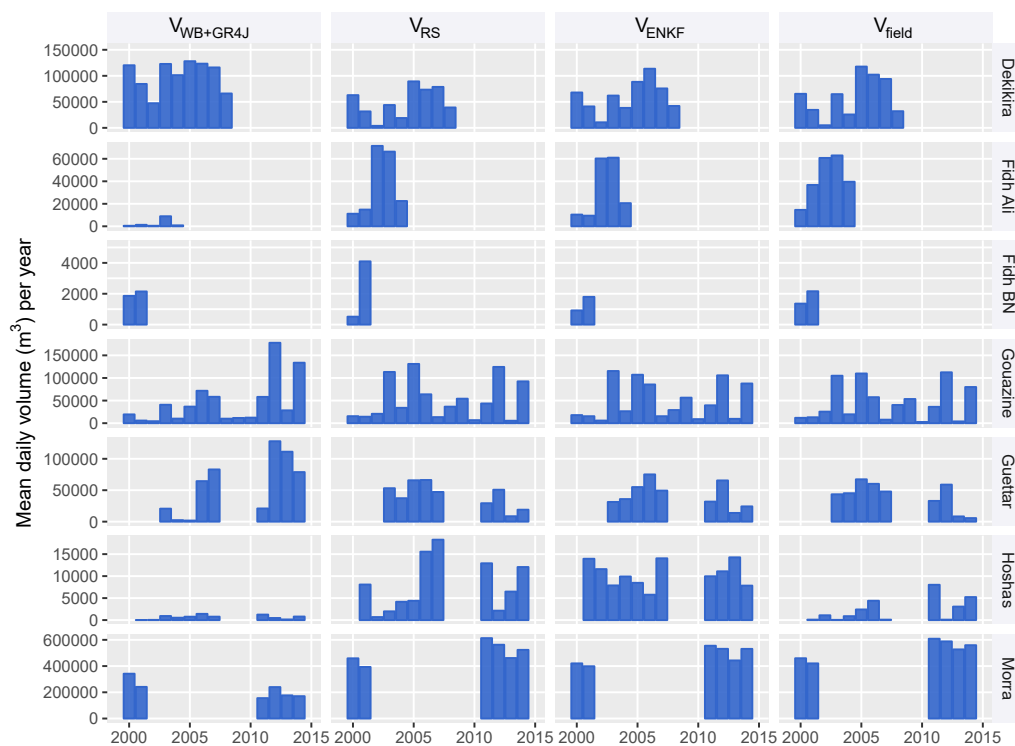


Fig. 10. Modelled and observed mean daily water volumes per year for all 7 lakes. Years with no field observations between 1999-2014 were excluded here.

Table 2: Ensemble Kalman Filter performance on daily volumes

Lakes (modelled period)	Initial capacity (10^3m^3)	NSE			RMSE (m^3)			NRMSE
		$V_{WB+GRAJ}$	V_{RS}	V_{ENKF}	$V_{WB+GRAJ}$	V_{RS}	V_{ENKF}	V_{ENKF}
Gouazine (1999-2014)	237	0.57	0.84	0.81	45200	25300	25900	0.09
Dekikira (1999-2008)	219	0.69	0.73	0.78	44000	25800	23700	0.13
Fidh Ali (1999-2005)	134	0.17	0.70	0.55	39200	20900	20900	0.24
Fidh Ben Nasseur (1999-2001)	47	0.45	0.11	0.44	6500	1500	6600	0.21
Morra (1999-2014)	705	0.12	0.62	0.46	274300	76400	90000	0.30
Hoshas (2001-2014)	130	0.48	0.02	0.02	3000	23400	23100	0.56
Guettar (2003-2014)	150	0.18	0.50	0.49	62500	31800	28300	0.25

472 much larger volumes on nearby lakes. Again, by modelling the decline be-
473 tween two Landsat observation and reducing certain outliers, the ENKF also
474 improved upon V_{RS} on certain lakes (e.g. Gouazine, Dekikira) but on others,
475 the poor initial forecast degraded the ENKF performance (e.g. Guettar and
476 Morra). Overall, ENKF displayed superior results than on individual values
477 due to the annual smoothing of observations, leading to very high levels of
478 NSE (0.99 across all lakes) and a mean RMSE (excluding the larger Morra
479 dam) reduced here to $10\,500\text{ m}^3$.

480 On Hoshas, $V_{WB+GRAJ}$ continued to perform better than V_{ENKF} despite
481 underestimating all events, due to the small and short floods experienced
482 which lead to a drastic, incorrect increase in water availability from single
483 remote sensing outliers. These were removed here through cloud and shadow
484 filtering and capping volume outputs to the known maximum capacities,
485 however residual outliers due to undetected cirrus clouds or shadows remain.

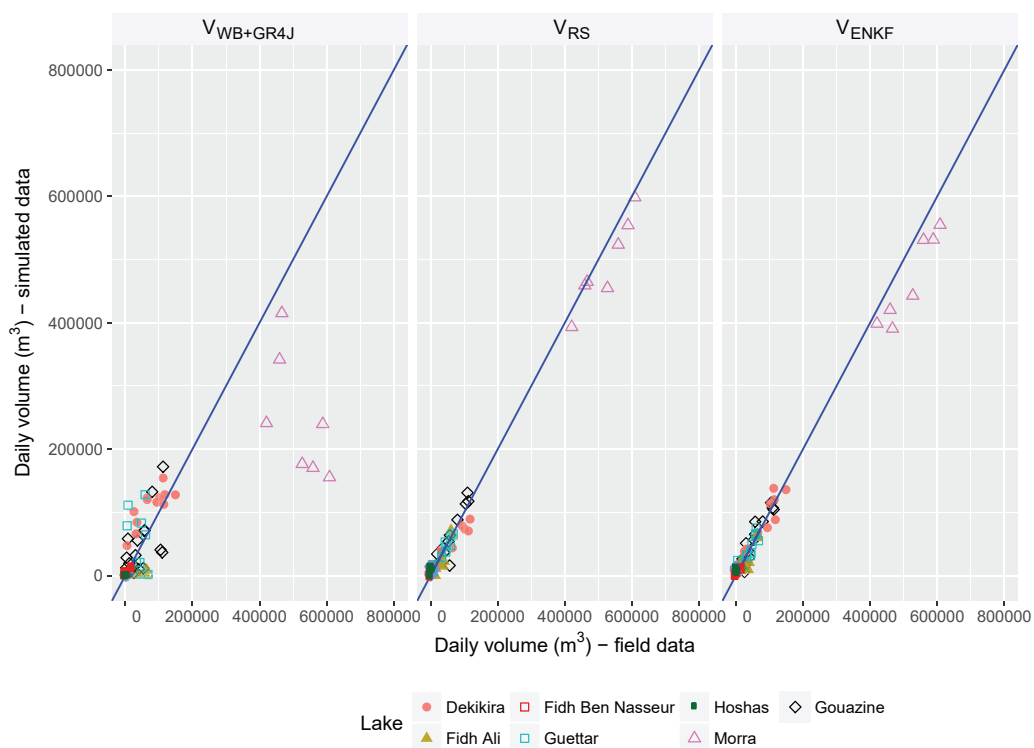


Fig. 11. Scatterplot between modelled and observed mean daily volumes per year for 7 lakes, 1999-2014

486 Improvements in the way clouds (especially cirrus clouds) are detected as well
487 as increased temporal and spatial accuracy will help reduce remote sensing
488 errors. Higher spatial resolution will increase precision, while more frequent
489 images will allow outliers to be corrected faster, reducing water availability
490 errors which depend on the lag between subsequent correct observations.
491 Improvements in the method may also be gained by defining specific Kalman
492 gain values for each RS observation to reflect for the presence of clouds at the
493 image level and the associated greater uncertainty over specific observations.

494 Interestingly, remote sensing uncertainties affected the smaller lakes (e.g.
495 Hoshas) where errors are proportionally more important but also lakes with
496 limited variation in surface area. On Morra for instance, the variations are
497 contained within the % error of surface area estimates from our MNDWI
498 method. Accordingly, on Morra ENKF outputs for individual observations
499 were heavily affected (NSE=0.46), but mean annual availability performed
500 well (NSE=0.89).

501 *3.3. Ensemble Kalman filter performance as data uncertainties rise*

502 Figure 12 and table 4 illustrate the difficulties in modelling daily flood
503 dynamics as uncertainties in the data inputs rise. In the absence of upstream
504 rainfall gauges, the performance of the hydrological model degraded (cf. sec-
505 tion 3.1.1) and RMSE rose by 28%. The ENKF however continues to improve
506 performance and correct for these errors, with NSE on daily volumes reduc-
507 ing marginally from 0.81 to 0.75. RMSE values for the daily observations
508 increase by 21% but remain 46 % lower than the initial WB+GR4J forecast
509 thanks to the remote sensing corrections. Using an average locally derived
510 infiltration rule based on 13 small reservoirs (Ogilvie, 2015) prevented the

Table 3: Ensemble Kalman Filter performance on mean annual water availability

Lakes (modelled period)	Mean daily volume (m ³)	NSE			RMSE (m ³)		
		$V_{WB+GRAJ}$	V_{RS}	V_{ENKF}	$V_{WB+GRAJ}$	V_{RS}	V_{ENKF}
Gouazine (1999-2014)	42800	0.38	0.87	0.89	36700	13500	11500
Dekikira (1999-2008)	59000	0.65	0.71	0.89	41600	20500	14500
Fidh Ali (1999-2005)	32200	0.09	0.52	0.60	35300	13500	12400
Fidh Ben Nasseur (1999-2001)	1000	0.66	0.67	NA	4300	2400	4400
Morra (1999-2014)	448900	0.40	0.89	0.89	304500	31700	55700
Hoshas (2001-2014)	800	0.37	0.11	0.09	2400	8700	9500
Guettar (2003-2014)	29000	0.09	0.88	0.74	56500	7100	10700

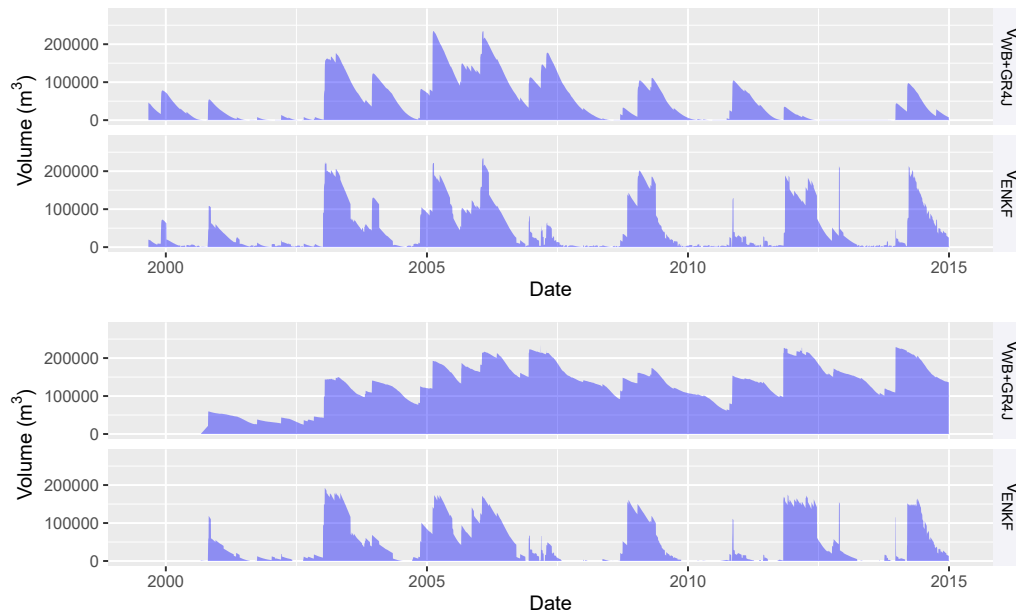


Fig. 12. Modelled daily volumes on Gouazine lake when degrading inputs. Top: with no rainfall gauge in the catchment. Bottom: with the average infiltration value from 15 reservoirs

511 model on Gouazine to reproduce the emptying of the lakes between succes-
512 sive events. This lead to a rising drift in volumes and RMSE values of the
513 $V_{WB+GR4J}$ initial forecast rising drastically to 97 000 m³. Again, the Kalman
514 filter using Landsat observations provided valuable corrections and RMSE
515 values on individual observations remained close (+ 15%) to those with the
516 site specific model. As the confidence in the model inputs & parameters (on
517 $I, P,$) degrades or significant additional fluxes can not be modelled reliably
518 (releases, withdrawals), the benefit of assimilation with remote sensing ob-
519 servations as expected increases. However the benefit of V_{ENKF} over simply
520 exploiting interpolated V_{RS} values also declines, due to the initial forecast
521 becoming so uncertain. RMSE on V_{RS} remains on average 18% lower than
522 V_{ENKF} in these four examples (table 4).

523 When considering ungauged catchments with no locally calibrated GR4J
524 parameters and no site specific HSV relation, the Kalman gain continues to
525 valuably correct the hydrological model's initial forecast, reducing RMSE by
526 30% (table 4). The increase in RMSE for V_{ENKF} is however amplified by
527 the uncertainties in V_{RS} , due to the surface-volume power relations used. A
528 locally derived power relation was shown to increase errors to near 40% on
529 Dekikira due to the difficulty in accounting for local lake morphologies and
530 the abrupt changes from silting (Ogilvie et al., 2016a). New techniques based
531 on high spatial resolution sensors open up increased possibilities to acquire at
532 lower costs (time, equipment) sufficient topographic detail to render surface
533 volumes rating curves (Avisse et al., 2017; Baup et al., 2014; van Bemmelen
534 et al., 2016; Massuel et al., 2014a) of multiple reservoirs of different geo-
535 morphology. Similarly, data assimilation with Landsat observations could be

Table 4: Kalman Filter performance on daily volumes when degrading model inputs and parameters

Lake	Degraded inputs	RMSE (m ³ /day)			RMSE increase (%)		
		$V_{WB+GRAJ}$	V_{RS}	V_{ENKF}	$V_{WB+GRAJ}$	V_{RS}	V_{ENKF}
Gouazine	Rainfall data	57800	25300	31400	+28%	+0%	+21%
Gouazine	Infiltration data	97000	25300	29800	+115%	+0%	+15%
Dekikira	GR4J parameters and HSV	52800	35800	38500	+20%	+39%	+63%
Fidh Ali	GR4J parameters and HSV	43000	20100	29000	+10%	-3%	+39%

536 used to calibrate over time the GR4J parameters, notably $X1$, based on the
537 estimated runoff. This approach was not explored here due to the rainfall
538 uncertainties observed at this sub basin scale and the temporal resolution of
539 Landsat imagery, which would lead to incorrect quantification of daily runoff
540 and thus calibration of the parameters.

541 4. Conclusions

542 Landsat surface water estimates coupled with an Ensemble Kalman Filter
543 showed their potential to improve hydrological modelling of small reservoirs.
544 Remote sensing observations provided vital corrections to the flood ampli-
545 tudes incorrectly estimated by the GR4J model which suffered notably from
546 rainfall detection issues. Conversely, site specific rules on depletion fluxes
547 (infiltration, withdrawals, etc.) led to an accurate modelling of the flood de-
548 cline, improving over interpolated Landsat observations, limited by reduced
549 temporal resolution. Overall performance reached high skill levels (NSE rose
550 from 0.64 to 0.94 on daily values) and RMSE reduced by two thirds down to
551 10 500 m³ when considering annual water availability.

552 Uncertainties from limited data availability (rainfall, infiltration, stage
553 data to calibrate P-Q models) were seen to increase the benefit of the ENKF
554 approach, but can also degrade the hydrological model to a point where it
555 becomes preferable to rely exclusively on interpolated Landsat surface area
556 observations. These performed well except on the smallest lakes, coherent
557 with the medium resolution imagery used here, and due to certain outliers
558 whose interpolation can reduce skill values over short periods. Time series
559 from the new generation of high temporal and spatial resolution satellite
560 imagery (e.g. Sentinel-2) are expected to further improve the accuracy of
561 remote sensing and associated data assimilation approaches on these smaller
562 reservoirs.

563 The Kalman filter approach may also be varied to seek to correct not
564 individual observations, but rather to estimate model inputs (e.g. rainfall) or
565 model parameters. This could notably be developed to improve hydrological
566 models on ungauged lakes, but would require frequent satellite observations,
567 close to flood peaks to provide sufficient accuracy in estimating daily runoff.
568 Similarly, over decline phases, where sufficient confidence in infiltration and
569 evaporation exists, the remote sensing observations could be used to identify
570 withdrawal rates. The ENKF method may also be enhanced by fine tuning
571 (Moradkhani et al., 2005) the covariances to compose with both sources of
572 uncertainty and provide greater confidence to remote sensing observations
573 over field data based on additional criteria (lake size, cloud presence across
574 image, etc.).

575 By drastically improving the performance of hydrological modelling in
576 data scarce semi-arid catchments, the Ensemble Kalman filter may improve

577 local water availability assessments (Wisser et al., 2010) but also provides
578 much needed data on the runoff captured by multiple reservoirs. These may
579 then serve as multiple runoff gauges to be integrated into larger scale models
580 (Gal et al., 2016; Liebe et al., 2009) and feed into the growing discussions
581 over their influence for downstream water users and uses.

582 **Acknowledgements**

583 We gratefully acknowledge the collaboration from the Direction Générale
584 de l'Aménagement et de la Conservation des Terres Agricoles (DG ACTA)
585 and Direction Générale des Ressources en Eau (DGRE) in Tunis and lo-
586 cal representatives at the Kairouan and Siliana Commissariat Régional au
587 Développement Agricole (CRDA). These works were partly financed by the
588 ANR AMETHYST and SICMED DYSHYME projects. Finally, we thank
589 the associate editor and two anonymous reviewers for their comments which
590 helped strengthen the manuscript.

591 **Appendix A. Supplementary materials**

Table A.1: Infiltration values (mm/day) for small reservoirs in and around the Merguellil upper catchment. Values for Fidh Ali, Fidh Ben Nasseur and Morra were adapted from Lacombe (2007)

Lake	Mean infiltration	Infiltration for Z_{min} (i_0)	Infiltration for Z_{max}	Infiltration rise per m (a^*1000)
Dekikira	2.7	2.70	2.7	0
Hoshas	28	3.62	77.1	24.50
Guettar	10	10.00	10.0	0
Gouazine	9	13.00	7.5	-1.38
Fidh Ali	3.6	3.60	3.6	0
Fidh Ben Nasseur	7.8	3.06	12.5	3.14
Morra	2	1.48	2.5	0.53

592 **References**

- 593 Alazard, M., Leduc, C., Travi, Y., Boulet, G., Ben Salem, A., 2015. Estimatif
594 ing evaporation in semi-arid areas facing data scarcity: Example of the El
595 Haouareb dam (Merguellil catchment, Central Tunisia). *J. Hydrol. Reg. Stud.* 3, 265–284. doi:10.1016/j.ejrh.2014.11.007.
596
- 597 Albergel, J., Moussa, R., Chahinian, N., 2003. Les processus hortonien et
598 leur importance dans la genèse et le développement des crues en zones
599 semi-arides. *La Houille Blanche*, 65–73.
- 600 Albergel, J., Rejeb, N., 1997. Les lacs collinaires en Tunisie : Enjeux, Con-
601 traintes et Perspectives. *C. R. Acad. Agric. Fr.* 83, 77–88.
- 602 Aouissi, J., Benabdallah, S., Lili Chabaâne, Z., Cudennec, C., 2018. Valu-
603 ing scarce observation of rainfall variability with flexible semi-distributed

- 604 hydrological modelling Mountainous Mediterranean context. *Sci. Total*
605 *Envir.* 643, 346–356. doi:10.1016/J.SCITOTENV.2018.06.086.
- 606 Avalos, J.E., 2004. Modélisation hydrologique globale conceptuelle appliquée
607 aux petits bassins versants en zone semi-aride du nord-Mexique. *Rev. Sci.*
608 *Eau* 17, 195–212. doi:10.7202/705530ar.
- 609 Avisse, N., Tilmant, A., Müller, M.F., Zhang, H., 2017. Monitoring small
610 reservoirs' storage with satellite remote sensing in inaccessible areas. *Hy-*
611 *drol. Earth Syst. Sci.* 21, 6445–6459. doi:10.5194/hess-21-6445-2017.
- 612 Baccari, N., Boussema, M., Lamachere, J., Nasri, S., 2008. Effi-
613 ciency of contour benches, filling-in and silting-up of a hillside reser-
614 voir in a semi-arid climate in Tunisia. *C. R. Geosci.* 340, 38–48.
615 doi:10.1016/j.crte.2007.09.020.
- 616 Baup, F., Frappart, F., Maubant, J., 2014. Combining high-resolution satel-
617 lite images and altimetry to estimate the volume of small lakes. *Hydrol.*
618 *Earth Syst. Sci.* 18, 2007–2020. doi:10.5194/hess-18-2007-2014.
- 619 van Bemmelen, C.W.T., Mann, M., de Ridder, M.P., Rutten, M.M., van de
620 Giesen, N.C., 2016. Determining water reservoir characteristics with global
621 elevation data. *Geophys. Res. Lett.* 43. doi:10.1002/2016GL069816.
- 622 Beven, K., Freer, J., 2001. Equifinality, data assimilation, and uncertainty
623 estimation in mechanistic modelling of complex environmental systems
624 using the GLUE methodology. *J. Hydrol.* 249, 11–29. doi:10.1016/S0022-
625 1694(01)00421-8.

- 626 Boulet, G., Kerr, Y., Chehbouni, A., Kalma, J.D., 2002. Deriving
627 catchment-scale water and energy balance parameters using data assimilation based on extended Kalman filtering. *Hydrol. Sci. J.* 47, 449–467.
628 doi:10.1080/02626660209492946.
629
- 630 Cadier, E., 1996. Hydrologie des petits bassins du Nordeste Brésilien
631 semi-aride: typologie des bassins et transposition écoulements annuels
632 Small watershed hydrology in semi-arid north-eastern Brazil: basin typology and transposition of annual runoff data. *J. Hydrol.* 182, 117–141.
633 doi:10.1016/0022-1694(95)02933-8.
634
- 635 Clark, M.P., Rupp, D.E., Woods, R.A., Zheng, X., Ibbitt, R.P., Slater, A.G.,
636 Schmidt, J., Uddstrom, M.J., 2008. Hydrological data assimilation with
637 the ensemble Kalman filter: Use of streamflow observations to update
638 states in a distributed hydrological model. *Adv. Water Resour.* 31, 1309–
639 1324. doi:10.1016/j.advwatres.2008.06.005.
- 640 Coron, L., Thirel, G., Delaigue, O., Perrin, C., Andréassian, V., 2017. The
641 suite of lumped GR hydrological models in an R package. *Environ. Model. Soft.* 94, 166–171. doi:10.1016/J.ENVSOF.2017.05.002.
642
- 643 Crétaux, J.F., Biancamaria, S., Arsen, A., Bergé-Nguyen, M., Becker, M.,
644 2015. Global surveys of reservoirs and lakes from satellites and regional
645 application to the Syrdarya river basin. *Environ. Res. Lett.* 10, 015002.
646 doi:10.1088/1748-9326/10/1/015002.
- 647 Cudennec, C., Leduc, C., Koutsoyiannis, D., 2007. Dryland hydrology

- 648 in Mediterranean regions - a review. *Hydrol. Sci. J.* 52, 1077–1087.
649 doi:10.1623/hysj.52.6.1077.
- 650 Desconnets, J., Taupin, J., Lebel, T., Leduc, C., 1997. Hydrology
651 of the HAPEX-Sahel Central Super-Site: surface water drainage and
652 aquifer recharge through the pool systems. *J. Hydrol.* 188-189, 155–178.
653 doi:10.1016/S0022-1694(96)03158-7.
- 654 Doumounia, A., Gosset, M., Cazenave, F., Kacou, M., Zougmore, F., 2014.
655 Rainfall monitoring based on microwave links from cellular telecommuni-
656 cation networks: First results from a West African test bed. *Geophys. Res.*
657 *Lett.* 41, 6016–6022. doi:10.1002/2014GL060724.
- 658 Emery, C.M., Paris, A., Biancamaria, S., Boone, A., Calmant, S., Garambois,
659 P.A., da Silva, J.S., 2017. Large scale hydrological model river storage
660 and discharge correction using satellite altimetry-based discharge product.
661 *Hydrol. Earth Syst. Sci. Discuss.*, 1–54. doi:10.5194/hess-2017-516.
- 662 Evensen, G., 2003. The Ensemble Kalman Filter: Theoretical for-
663 mulation and practical implementation. *Ocean Dyn.* 53, 343–367.
664 doi:10.1007/s10236-003-0036-9.
- 665 Feki, H., Slimani, M., Cudennec, C., 2012. Incorporating elevation in rainfall
666 interpolation in Tunisia using geostatistical methods. *Hydrol. Sci. J.* 57,
667 1294–1314. doi:10.1080/02626667.2012.710334.
- 668 Feng, M., Sexton, J.O., Channan, S., Townshend, J.R., 2016. A global,
669 high-resolution (30-m) inland water body dataset for 2000: first results

- 670 of a topographic-spectral classification algorithm. *Int. J. Digit. Earth* 9,
671 113–133. doi:10.1080/17538947.2015.1026420.
- 672 Forkel, M., Carvalhais, N., Verbesselt, J., Mahecha, M., Neigh, C., Reich-
673 stein, M., 2013. Trend Change Detection in NDVI Time Series: Effects
674 of Inter-Annual Variability and Methodology. *Remote Sens.* 5, 2113–2144.
675 doi:10.3390/rs5052113.
- 676 Frappart, F., Biancamaria, S., Normandin, C., Blarel, F., Bourrel, L.,
677 Aumont, M., Azemar, P., Vu, P.L., Le Toan, T., Lubac, B., Dar-
678 rozes, J., 2018. Influence of recent climatic events on the surface wa-
679 ter storage of the Tonle Sap Lake. *Sci. Total Environ.* 636, 1520–1533.
680 doi:10.1016/J.SCITOTENV.2018.04.326.
- 681 Gal, L., Grippa, M., Hiernaux, P., Peugeot, C., Mougin, E., Kergoat, L.,
682 2016. Changes in lakes water volume and runoff over ungauged Sahelian
683 watersheds. *J. Hydrol.* 540, 1176–1188. doi:10.1016/j.jhydrol.2016.07.035.
- 684 Gao, P., Mu, X.M., Wang, F., Li, R., 2011. Changes in streamflow and sedi-
685 ment discharge and the response to human activities in the middle reaches
686 of the Yellow River. *Hydrol. Earth Syst. Sci.* 15, 1–10. doi:10.5194/hess-
687 15-1-2011.
- 688 Gillijns, S., Mendoza, O., Chandrasekar, J., De Moor, B., Bernstein, D.,
689 Ridley, A., 2006. What is the ensemble Kalman filter and how well
690 does it work?, in: *American Control Conference 2006, IEEE.* p. 6.
691 doi:10.1109/ACC.2006.1657419.

- 692 Grunberger, O., Montoroi, J., Nasri, S., 2004. Quantification of water ex-
693 change between a hill reservoir and groundwater using hydrological and
694 isotopic modelling (El Gouazine, Tunisia). *C. R. Geosci.* 336, 1453–1462.
695 doi:10.1016/j.crte.2004.08.006.
- 696 He, X., Li, Z., Hao, M., Tang, K., Zheng, F., 2003. Down-scale analysis for
697 water scarcity in response to soil -water conservation on Loess Plateau
698 of China. *Agric. Ecosyst. Environ.* 94, 355–361. doi:10.1016/S0167-
699 8809(02)00039-7.
- 700 Hengl, T., Heuvelink, G.B., Rossiter, D.G., 2007. About regression-
701 kriging: From equations to case studies. *Comput. Geosci.* 33, 1301–1315.
702 doi:10.1016/j.cageo.2007.05.001.
- 703 Hentati, A., Kawamura, A., Amaguchi, H., Iseri, Y., 2010. Evaluation of
704 sedimentation vulnerability at small hillside reservoirs in the semi-arid
705 region of Tunisia using the Self-Organizing Map. *Geomorphology* 122,
706 56–64. doi:10.1016/j.geomorph.2010.05.013.
- 707 Hrachowitz, M., Savenije, H., Blöschl, G., McDonnell, J., Sivapalan, M.,
708 Pomeroy, J., Arheimer, B., Blume, T., Clark, M., Ehret, U., Fenicia, F.,
709 Freer, J., Gelfan, A., Gupta, H., Hughes, D., Hut, R., Montanari, A.,
710 Pande, S., Tetzlaff, D., Troch, P., Uhlenbrook, S., Wagener, T., Win-
711 semius, H., Woods, R., Zehe, E., Cudennec, C., 2013. A decade of Predic-
712 tions in Ungauged Basins (PUB)a review. *Hydrol. Sci. J.* 58, 1198–1255.
713 doi:10.1080/02626667.2013.803183.
- 714 Kingumbi, A., Bargaoui, Z., Ledoux, E., Besbes, M., Hubert, P., 2007.

- 715 Modélisation hydrologique stochastique d'un bassin affecté par des change-
716 ments d'occupation: cas du Merguellil en Tunisie centrale. *Hydrol. Sci. J.*
717 52, 1232–1252. doi:10.1623/hysj.52.6.1232.
- 718 Lacombe, G., 2007. Evolution et usages de la ressource en eau dans un
719 bassin versant aménagé semi-aride. Le cas du Merguellil en Tunisie Cen-
720 trale. Ph.D. thesis. Université Montpellier II.
- 721 Lacombe, G., Cappelaere, B., Leduc, C., 2008. Hydrological impact of water
722 and soil conservation works in the Merguellil catchment of central Tunisia.
723 *J. Hydrol.* 359, 210–224. doi:10.1016/j.jhydrol.2008.07.001.
- 724 Leauthaud, C., Belaud, G., Duvail, S., Moussa, R., Grünberger, O., Albergel,
725 J., 2013. Characterizing floods in the poorly gauged wetlands of the Tana
726 River Delta, Kenya, using a water balance model and satellite data. *Hydrol.*
727 *Earth Syst. Sci.* 17, 3059–3075. doi:10.5194/hess-17-3059-2013.
- 728 Leduc, C., Ben Ammar, S., Favreau, G., Beji, R., Virrion, R., Lacombe,
729 G., Tarhouni, J., Aouadi, C., Zenati Chelli, B., Jebnoun, N., Oi, M.,
730 Michelot, J., Zouari, K., 2007. Impacts of hydrological changes in the
731 Mediterranean zone: environmental modifications and rural development
732 in the Merguellil catchment, central Tunisia. *Hydrol. Sci. J.* 52, 1162–1178.
733 doi:10.1623/hysj.52.6.1162.
- 734 Lehner, B., Liermann, C.R., Revenga, C., Vörösmarty, C., Fekete, B.,
735 Crouzet, P., Döll, P., Endejan, M., Frenken, K., Magome, J., Nilsson, C.,
736 Robertson, J.C., Rödel, R., Sindorf, N., Wisser, D., 2011. High-resolution

- 737 mapping of the world's reservoirs and dams for sustainable river-flow man-
738 agement. *Front. Ecol. Environ.* 9, 494–502. doi:10.1890/100125.
- 739 Li, Q., Gowing, J., 2005. A Daily Water Balance Modelling Approach for
740 Simulating Performance of Tank-Based Irrigation Systems. *Water Resour.*
741 *Manag.* 19, 211–231. doi:10.1007/s11269-005-2702-9.
- 742 Liebe, J., van de Giesen, N., Andreini, M., 2005. Estimation of small reservoir
743 storage capacities in a semi-arid environment. *Phys. Chem. Earth, Parts*
744 *A/B/C* 30, 448–454. doi:10.1016/j.pce.2005.06.011.
- 745 Liebe, J.R., van de Giesen, N., Andreini, M., Walter, M.T., Steenhuis, T.S.,
746 2009. Determining watershed response in data poor environments with
747 remotely sensed small reservoirs as runoff gauges. *Water Resour. Res.* 45,
748 W07410. doi:10.1029/2008WR007369.
- 749 Linacre, E., 1994. Estimating U.S. Class A Pan Evaporation from Few Cli-
750 mate Data. *Water Int.* 19, 5–14. doi:10.1080/02508069408686189.
- 751 Ma, H., Yang, D., Tan, S.K., Gao, B., Hu, Q., 2010. Impact of climate vari-
752 ability and human activity on streamflow decrease in the Miyun Reservoir
753 catchment. *J. Hydrol.* 389, 317–324. doi:10.1016/j.jhydrol.2010.06.010.
- 754 Martin-Rosales, W., Leduc, C., 2003. Dynamiques de vidange d'une mare
755 temporaire au Sahel : l'exemple de Banizoumbou (Sud-Ouest du Niger).
756 *C. R. Geosci.* 335, 461–468. doi:10.1016/S1631-0713(03)00059-2.
- 757 Massuel, S., Feurer, D., Ogilvie, A., Calvez, R., Rochette, R., 2014a.
758 Vers l'amélioration du bilan hydrologique des retenues collinaires par la

- 759 prise de vue aéroportée légère, in: Drones et moyens légers aéroportés
760 d'observation, Montpellier, France. p. 1.
- 761 Massuel, S., Perrin, J., Mascré, C., Mohamed, W., Boisson, A., Ahmed,
762 S., 2014b. Managed aquifer recharge in South India: What to expect
763 from small percolation tanks in hard rock? *J. Hydrol.* 512, 157–167.
764 doi:10.1016/j.jhydrol.2014.02.062.
- 765 McMahon, T.A., Peel, M.C., Lowe, L., Srikanthan, R., McVicar, T.R., 2013.
766 Estimating actual, potential, reference crop and pan evaporation using
767 standard meteorological data: a pragmatic synthesis. *Hydrol. Earth Syst.*
768 *Sci.* 17, 1331–1363. doi:10.5194/hess-17-1331-2013.
- 769 Molle, F., 1991. Caractéristiques et potentialités des Açudes du nord-est
770 brésilien. Ph.D. thesis. Université de Montpellier 2, France.
- 771 Montoroi, J.P., Grunberger, O., Nasri, S., 2002. Groundwater geochemistry
772 of a small reservoir catchment in Central Tunisia. *Appl. Geochem.* 17,
773 1047–1060. doi:10.1016/S0883-2927(02)00076-8.
- 774 Moradkhani, H., Sorooshian, S., Gupta, H.V., Houser, P.R., 2005.
775 Dual state - parameter estimation of hydrological models us-
776 ing ensemble Kalman filter. *Adv. Water. Resour.* 28, 135–147.
777 doi:10.1016/j.advwatres.2004.09.002.
- 778 Moussa, R., 2010. When monstrosity can be beautiful while normality can
779 be ugly: assessing the performance of event-based flood models. *Hydrol.*
780 *Sci. J.* 55, 1074–1084. doi:10.1080/02626667.2010.505893.

- 781 Mu, Q., Zhao, M., Running, S.W., 2011. Improvements to a MODIS global
782 terrestrial evapotranspiration algorithm. *Remote Sens. Environ.* 115, 1781–
783 1800. doi:10.1016/j.rse.2011.02.019.
- 784 Mueller, N., Lewis, A., Roberts, D., Ring, S., Melrose, R., Sixsmith, J.,
785 Lymburner, L., McIntyre, A., Tan, P., Curnow, S., Ip, A., 2016. Wa-
786 ter observations from space: Mapping surface water from 25 years of
787 Landsat imagery across Australia. *Remote Sens. Environ.* 174, 341–352.
788 doi:10.1016/j.rse.2015.11.003.
- 789 Nasri, S., 2007. Caractéristiques et impacts hydrologiques de banquettes en
790 cascade sur un versant semi-aride en Tunisie centrale. *Hydrol. Sci. J.* 52,
791 1134–1145. doi:10.1623/hysj.52.6.1134.
- 792 Neppel, L., Desbordes, M., Masson, J.M., 1998. Influence de l'évolution
793 dans l'espace et le temps d'un réseau de pluviomètres sur l'observation
794 des surfaces de pluie en fonction de leur aire. *Rev. Sci. Eau* 11, 43–60.
795 doi:10.7202/705296ar.
- 796 Nyssen, J., Clymans, W., Descheemaeker, K., Poesen, J., Vandecasteele, I.,
797 Vanmaercke, M., Zenebe, A., Van Camp, M., Haile, M., Haregeweyn, N.,
798 Moeyersons, J., Martens, K., Gebreyohannes, T., Deckers, J., Walraevens,
799 K., 2010. Impact of soil and water conservation measures on catchment
800 hydrological response-a case in north Ethiopia. *Hydrol. Process.* 24, 1880–
801 1895. doi:10.1002/hyp.7628.
- 802 Ogilvie, A., 2015. Upscaling water availability and water use assessments in
803 hydro-sociosystems: the small reservoirs of the Merguellil catchment (Cen-

- 804 tral Tunisia). Ph.D. thesis. Université de Montpellier and King's College
805 London.
- 806 Ogilvie, A., Belaud, G., Deleenne, C., Bailly, J.S., Bader, J.C., Oleksiak,
807 A., Ferry, L., Martin, D., 2015. Decadal monitoring of the Niger Inner
808 Delta flood dynamics using MODIS optical data. *J. Hydrol.* 523, 368–383.
809 doi:10.1016/j.jhydrol.2015.01.036.
- 810 Ogilvie, A., Belaud, G., Massuel, S., Mulligan, M., Le Goulven, P.,
811 Calvez, R., 2016a. Assessing Floods and Droughts in Ungauged
812 Small Reservoirs with Long-Term Landsat Imagery. *Geosciences* 6, 42.
813 doi:10.3390/GEOSCIENCES6040042.
- 814 Ogilvie, A., Le Goulven, P., Leduc, C., Calvez, R., Mulligan, M.,
815 2016b. Réponse hydrologique d'un bassin semi-aride aux événements plu-
816 viométriques et aménagements de versant (bassin du Merguellil, Tunisie
817 centrale). *Hydrol. Sci. J.* 61, 441–453. doi:10.1080/02626667.2014.934249.
- 818 Ogilvie, A., Belaud, G., Massuel, S., Mulligan, M., Le Goulven, P., Calvez,
819 R., 2018. Surface water monitoring in small water bodies: potential and
820 limits of multi-sensor Landsat time series. *Hydrol. Earth Syst. Sci. Discuss.*
821 1–35. doi:10.5194/hess-2018-19.
- 822 Oubanas, H., Gejadze, I., Malaterre, P.O., Mercier, F., 2018. River dis-
823 charge estimation from synthetic SWOT-type observations using varia-
824 tional data assimilation and the full Saint-Venant hydraulic model. *J.*
825 *Hydrol.* doi:10.1016/J.JHYDROL.2018.02.004.

- 826 Overeem, A., Leijnse, H., Uijlenhoet, R., 2013. Country-wide rainfall maps
827 from cellular communication networks. *Proc. Natl. Acad. Sci. U.S.A.* 110,
828 2741–5. doi:10.1073/pnas.1217961110.
- 829 Pekel, J.F., Cottam, A., Gorelick, N., Belward, A.S., 2016. High-resolution
830 mapping of global surface water and its long-term changes. *Nature* 540,
831 418–422. doi:10.1038/nature20584.
- 832 Perrin, C., Michel, C., Andréassian, V., 2003. Improvement of a par-
833 simonious model for streamflow simulation. *J. Hydrol.* 279, 275–289.
834 doi:10.1016/S0022-1694(03)00225-7.
- 835 Reichle, R.H., McLaughlin, D.B., Entekhabi, D., 2002. Hydrologic Data
836 Assimilation with the Ensemble Kalman Filter. *Mon. Weather Rev.* 130,
837 103–114. doi:10.1175/1520-0493(2002)130<0103:HDAWTE>2.0.CO;2.
- 838 Riou, C., 1972. Etude de l'évaporation en Afrique centrale. *Cahiers Orstom*,
839 Série Hydrologie, 39–52.
- 840 Sawunyama, T., Senzanje, A., Mhizha, A., 2006. Estimation of small
841 reservoir storage capacities in Limpopo River Basin using geographical
842 information systems (GIS) and remotely sensed surface areas: Case of
843 Mzingwane catchment. *Phys. Chem. Earth, Parts A/B/C* 31, 935–943.
844 doi:10.1016/j.pce.2006.08.008.
- 845 da Silva, J.S., Calmant, S., Seyler, F., Moreira, D.M., Oliveira, D., Monteiro,
846 A., 2014. Radar Altimetry Aids Managing Gauge Networks. *Water Resour.*
847 *Manag.* 28, 587–603. doi:10.1007/s11269-013-0484-z.

- 848 Soti, V., Puech, C., Lo Seen, D., Bertran, A., Vignolles, C., Mondet, B.,
849 Dessay, N., Tran, A., 2010. The potential for remote sensing and hydrologic
850 modelling to assess the spatio-temporal dynamics of ponds in the Ferlo Re-
851 gion (Senegal). *Hydrol. Earth Syst. Sci.* 14, 1449–1464. doi:10.5194/hess-
852 14-1449-2010.
- 853 Swenson, S., Wahr, J., 2009. Monitoring the water balance of
854 Lake Victoria, East Africa, from space. *J. Hydrol.* 370, 163–176.
855 doi:10.1016/j.jhydrol.2009.03.008.
- 856 Van Der Heijden, S., Haberlandt, U., 2010. Influence of spatial interpolation
857 methods for climate variables on the simulation of discharge and nitrate
858 fate with SWAT. *Adv. Geosci.* 27, 91–98. doi:10.5194/adgeo-27-91-2010.
- 859 Vermeulen, P.T.M., Heemink, A.W., 2006. Model-Reduced Varia-
860 tional Data Assimilation. *Mon. Weather Rev.* 134, 2888–2899.
861 doi:10.1175/MWR3209.1.
- 862 Wackernagel, H., 2004. Géostatistique et assimilation séquentielle de
863 données. H.D.R. Université Pierre et Marie Curie, France.
- 864 Wisser, D., Frohking, S., Douglas, E.M., Fekete, B.M., Schumann, A.H.,
865 Vörösmarty, C.J., 2010. The significance of local water resources captured
866 in small reservoirs for crop production - A global-scale analysis. *J. Hydrol.*
867 384, 264–275. doi:10.1016/j.jhydrol.2009.07.032.
- 868 Xie, X., Zhang, D., 2010. Data assimilation for distributed hydrological
869 catchment modeling via ensemble Kalman filter. *Adv. Water. Resour.* 33,
870 678–690. doi:10.1016/j.advwatres.2010.03.012.

- 871 Xu, H., 2006. Modification of normalised difference water index (NDWI) to
872 enhance open water features in remotely sensed imagery. *Int. J. Remote*
873 *Sens.* 27, 3025–3033. doi:10.1080/01431160600589179.
- 874 Yamazaki, D., Trigg, M.A., 2016. Hydrology: The dynamics of Earth’s
875 surface water. *Nature* 540, 348–349. doi:10.1038/nature21100.
- 876 Zammouri, M., Feki, H., 2005. Managing releases from small upland reser-
877 voirs for downstream recharge in semi-arid basins (Northeast of Tunisia).
878 *J. Hydrol.* 314, 125–138. doi:10.1016/j.jhydrol.2005.03.011.
- 879 Zribi, M., Chahbi, A., Shabou, M., Lili-Chabaane, Z., Duchemin, B., Bagh-
880 dadi, N., Amri, R., Chehbouni, A., 2011. Soil surface moisture estimation
881 over a semi-arid region using ENVISAT ASAR radar data for soil evapo-
882 ration evaluation. *Hydrol. Earth Syst. Sci.* 15, 345–358. doi:10.5194/hess-
883 15-345-2011.